Mechatronic Systems and Control, Vol. 54, No. 10, 2026
An Open Access Paper

ADAPTIVE PI-BASED SLIDING-MODE CONTROL FOR PLANT PROTECTION QUADROTORS WITH VARIABLE MASS AND SLOSHING

Shibbir Ahmed,[*,†] Muhammad Yousaf Nadeem,[*,†] Muhammad Zain,[**] Zubair Iqbal,[***] Issac Tawiah,[****] and Chengming Sun[*]

Abstract

The stability of autonomous liquid transporter unmanned aerial vehicles (UAVs) is crucial for precision in agricultural field spraying. This paper proposes an adaptive robust control scheme designed to stabilise agricultural quadrotor UAVs affected by variable mass and liquid sloshing dynamics during pesticide application. A comprehensive nonlinear mathematical model is developed to explicitly represent UAV–liquid interactions, accounting for both liquid sloshing and time-dependent mass variations. An adaptive PI-based sliding-mode controller is proposed, featuring a neural network identifier to estimate unknown sloshing forces and a nonlinear disturbance observer to mitigate external disturbances. Theoretical analysis through designed Lyapunov functions confirms the closed-loop system's robustness, stability, and bounded estimation errors, even despite varying liquid mass conditions. Simulation experiments validate the effectiveness of the proposed method, achieving approximately 41.4% and 53.8% in trajectory tracking accuracy, stabilisation, and disturbance rejection along the x- and y-axes, respectively, compared to the conventional proportional integral derivative (PID) counterpart. Overall, this research enhances UAV control methodologies by effectivelymanaging sloshing-induced dynamics, thereby facilitating improved quadrotor system designs and making a substantial contribution to agricultural automation.

Key Words

Agricultural sprayer UAVs, variable mass, liquid slosh, PID, sliding-mode controller, attitude tracking

1. Introduction

Unmanned aerial vehicles (UAVs), particularly quadrotors, have become fundamental across many sectors due to their agility and low operating costs. Ensuring stability under actuator faults and coping with adaptive control challenges has become a dominant research focus [1]–[3]. In agriculture, plant-protection UAVs are increasingly deployed for spraying and crop monitoring at low altitudes and near-canopy conditions [4]. Their missions are highly exposed to gusts and turbulence, demanding robust attitude stabilisation and precise position tracking [5]. Spraying outcomes – droplet size spectrum, deposition, and uniformity – are highly dependent on vehicle's flight dynamics and height/velocity control [6], [7]. Critically, the onboard liquid tank introduces continuous mass variations and sloshing-induced internal disturbances [8]. These effects shift the UAV's centre of mass and generate unmodelled, state-dependent forces and torques, thereby negatively impacting stability and tracking. Consequently, for fluid-carrying agricultural UAVs, there is a clear need for advanced dynamic models that include sloshing and time-varying mass, together with robust/adaptive controllers capable of estimating and compensating these effects in real time.

In both research and industry, early quadrotor controllers primarily relied on classical/linear approaches. For example, Tayebi and McGilvray [9] proposed a proportional–derivative (PD) law that achieves exponential attitude stabilisation, and subsequent research extended this baseline. Kendoul *et al.* [10] proposed a two-loop linear architecture that decouples inner-loop rotation from outer-loop translation to improve

[*] Key Laboratory of Crop Genetics and Physiology of Jiangsu Province, Key Laboratory of Crop Cultivation and Physiology of Jiangsu Province, College of Agriculture, Yangzhou University, Yangzhou 225009, China; e-mail: shibbir7ahmed@gmail.com; 008625@yzu.edu.cn; cmsun@yzu.edu.cn
[**] College of Water Conservancy, North China University of Water Resources and Electric Power, Zhengzhou 450046, China; e-mail: mzain113@outlook.com
[***] School of Science and the Environment, Memorial University of Newfoundland, St. John's, NL A1C 5S7, Canada; e-mail: ziqbal@mun.ca
[****] Department of Automation, Shanghai Jiao Tong University, Shanghai 200240, China; e-mail: isaac_k_tawiah@sjtu.edu.cn
[†] Shibbir Ahmed and Muhammad Yousaf Nadeem contributed equally to the work.
Corresponding author: Chengming Sun

Recommended by Min Xia
(DOI: 10.2316/J.2026.201-0597)

trajectory tracking performance. Building on these, Jiao *et al.* [11] developed a self-tuning linear active disturbance rejection controller (LADRC) using expert-rule-based gain adaptation and validated strong disturbance rejection in real flight. However, proportional–integral–derivative (PID) and other linear schemes degrade under lumped uncertainties and wind gusts [12], thereby motivating nonlinear methods. To address these issues, Madani and Benallegue [13] presented a backstepping controller for quadrotor/helicopter stabilisation, while Fresk and Nikolakopoulos [14] designed a quaternion-based attitude controller that avoids singularities. Likewise, Boudjedir *et al.* [15] presented a neural-network adaptive law for unknown system dynamics, and Wang *et al.* [16] achieved robust SO(3) attitude tracking through a variation-based linearisation combined with an interval-matrix approach.

A complementary development line focused on disturbance observer (DO)-based compensation to estimate and cancel unknown inputs in real time. Chen and Chen [17] designed a DO-based sliding-mode controller (SMC) for uncertain nonlinear systems and proved robust disturbance rejection through an integrated observer–controller pair. Through this concept, Tripathi *et al.* [18] proposed an intelligent finite-time SMC with a DO for quadrotors; Maqsood and Qu [19] implemented a nonlinear DO + SMC for quadrotor helicopters; and Izadi and Faieghi [20] developed a high-gain DO to achieve robust trajectory tracking. In related applications, Chen *et al.* [21] designed a DO-based compensation law using quantum-information concepts, while Diao *et al.* [22] achieved output-feedback altitude/attitude tracking under parametric uncertainty and unknown disturbances, also introducing adaptive approximation. Furthermore, Zhang *et al.* [23] handled time-varying, and nonvanishing disturbance classes in quadrotor rotational control, expanding DO theory to more tricky and practical dynamic conditions.

Building on rotation control under time-varying, non-vanishing disturbances in [23], Yang *et al.* [24] designed a variable-structure attitude controller effective in handling parameter uncertainty and external disturbances, yet but still assumes a rigid, constant-mass airframe. To capture mass shifts in special operations, Zhang *et al.* [25] modelled multi-factor coupling in heavy-equipment airdrop representing an abrupt mass and centre of gravity (CoG) change scenario. Conversely, for sustained mass-transfer tasks, Pedro *et al.* [26] developed a nonlinear dynamic inversion neurocontroller for aerial refueling, effectively addressing mass increase and CoG migration within a mission-specific regime. Closer to liquid payloads, Soltani and Vahidi Bajestani [27] proposed an LQG slosh-mitigation scheme using a single-mode equivalent slosh model linearised near hover along with an observer to estimate liquid states; however, it does not co-model continuous spray–drain mass change nor provide nonlinear/adaptive robustness. Complementarily, Wu *et al.* [28] modelled time-varying mass for a quadrotor and designed an SMC attitude tracker on a rigid-body plant (no slosh forces/moments), lacking online identification or a DO capability.

Although modelling and high-performance control of time-varying-mass quadrotors have been widely studied, two key limitations persist: (i) the disturbances induced by continuous mass change (and especially by internal liquid motion) are often not explicitly modelled/compensated and (ii) many established models fail to capture the coupled dynamics of mass variation and sloshing with sufficient fidelity, limiting their utility in real-world spraying operations. To address these challenges, the main contributions of this paper focus on the following three aspects:

(1) *Coupled Model:* A control-oriented 6-DOF model that embeds time-varying mass and sloshing-induced forces and moments directly in both the translational and rotational equations of motion.
(2) *AIPI-SMC:* An adaptive PI-based integral SMC tailored to agricultural spraying, combining a neural-network identifier (to learn residual slosh effects online) with a nonlinear DO (to reject external lumped disturbances), with Lyapunov-based uniformly ultimately bounded (UUB) guarantees.
(3) *Quantitative Gains:* Simulations under slosh + mass-drain show improved tracking, faster settling, and stronger disturbance rejection than a well-tuned PID baseline.

2. Mathematical Modelling

The primary structural difference between conventional survey quadrotors and agricultural sprayer UAVs lies in the integration of a liquid tank and the resulting sloshing dynamics. These elements significantly modify the quadrotor's dynamics behaviour, presenting distinct control and flight stability challenges. The liquid payload's time-varying mass and its unsteady sloshing motion exert a substantial effect on UAV flight stability and control precision. As the fluid is discharged during spraying, the UAV's total mass and centre of mass vary continuously change, altering aerodynamic forces and making accurate trajectory tracking more difficult. Furthermore, the oscillatory motion from liquid sloshing introduces additional nonlinear forces and moments, which further degrade UAV's stability and performance.

Let $\{F_I O_I, X_I, Y_I, Z_I\}$ denote the Earth-fixed inertial frame and $\{F_B O_B, X_B, Y_B, Z_B\}$ the body-fixed frame. The total UAV mass is $M = M_q + M_l(t)$, where $M_q \in \mathbb{R}$ is the quadrotor's mass, and $r_{\mathrm{ql}} \in \mathbb{R}^3$ connects the UAV's and liquid's centres of mass, influencing angular momentum (Fig. 1).

2.1 The Translational Motion

Let R be the rotation matrix from the inertial frame F_I to the body-fixed frame F_B, and $r_I \in \mathbb{R}^3$ the UAV's centre of mass in F_I. Neglecting Earth's rotation [10], the kinematic model is:

$$\dot{r}_I = R^T V_b^I = R^T V_b + (\omega_I \times r_I) \tag{1}$$

where V_b^I is the absolute velocity in F_B, V_b is its relative velocity, and ω_I is the angular velocity in F_I.

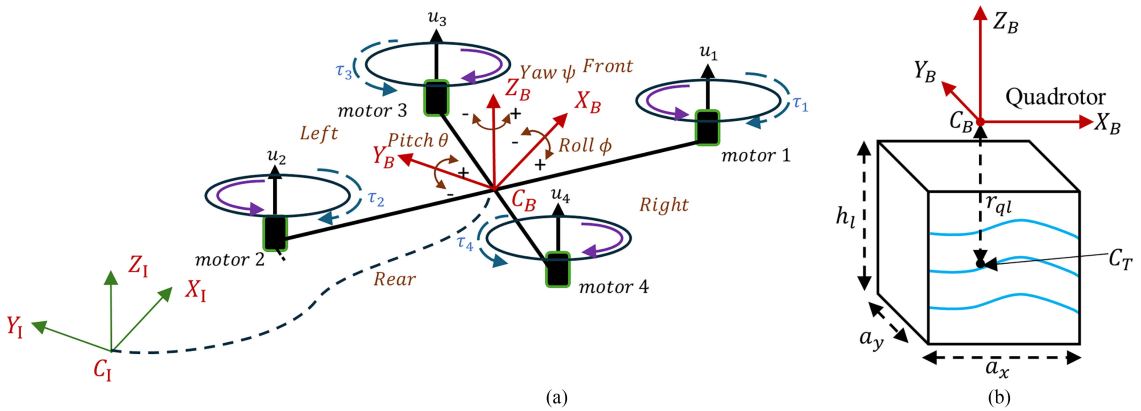

Figure 1. (a) The physical coordinate system of the UAV. (b) Liquid tank position and attachment.

Using Newton's second law for a system with time-varying mass [27]:

$$F_b + RMg = \frac{d\left(MV_b^I\right)}{dt_I} \tag{2}$$

With $M = M_q + m_l(t)$, the total mass. Applying the Coriolis formulation [26] and simplifying:

$$\begin{aligned}\dot{V}_b &= \frac{F_b}{M_q+m_l(t)} - \frac{\dot{m}_l(t)}{M_q+m_l(t)}\left[V_b + R\left(\omega_I \times r_I\right)\right] \\ &\quad - \left(\omega_b + R\omega_I\right) \times V_b + R\left[g - \omega_I \times \left(\omega_I \times r_I\right)\right]\end{aligned} \tag{3}$$

Equation (3) captures the translational dynamics, including time-varying mass and inertial coupling terms. It is observed that if $\dot{m}_l(t)$ is negligible, then $\dot{V}_b$ approaches the fixed mass version of the quadrotor. In this case, the net force F_b includes external forces F_{ext} and internal forces F_{in}, such that $F_b = F_{\text{ext}} + F_{\text{in}}$. The external forces consist of the thrust F_t and other forces F_0: $F_{\text{ext}} = F_t + F_0$, where $F_t = \begin{bmatrix}0 & 0 & -\sum_{i=1}^{4} F_{t_i}\end{bmatrix}^T \in \mathbb{R}^3$, with F_{t_i} being the thrust from the rotor i. For the internal forces, although other forces like viscosity can be considered, the sloshing force F_s is regraded for the sprayer quadrotor; thus, $F_{\text{in}} = F_s$.

2.1.1 Modelling Sloshing Effect

The sloshing force components [26] during UAV manoeuvres can be expressed as:

$$F_{\text{sx}} = -\rho \sum_{i=1}^{\infty}\sum_{j=0}^{\infty} \ddot{\beta}_{\text{ij}}(t)\,\lambda_{\text{xij}}, \tag{4}$$

$$F_{\text{sy}} = -\rho \sum_{j=0}^{\infty} \ddot{\beta}_{0j}(t)\,\lambda_{y0j} \tag{5}$$

With ρ the fluid density, and λ_{xij} and λ_{y0j} are hydrodynamic coefficients. Under free oscillations, $\beta_{\text{ij}}(t)$ can be modelled as a harmonic function:

$$\beta_{\text{ij}}(t) = \bar{\beta}_{\text{ij}} \sin\left(\omega_{\text{ij}} t\right) \tag{6}$$

where $\bar{\beta}_{\text{ij}}$ is the amplitude of the sloshing mode (i, j), and ω_{ij} is the sloshing frequency of the mode (i, j). Similarly, the sloshing moments are computed as:

$$\Omega_{\text{sx}} = \rho \text{R} \sum_{j=1}^{\infty} \ddot{\beta}_{\text{oj}}(t) \tag{7}$$

$$,\Omega_{\text{sy}} = -\rho \sum_{i=1}^{\infty}\sum_{j=1}^{\infty} \frac{\ddot{\beta}_{\text{ij}}(t)}{\mathcal{K}_{\text{ij}}} \tag{8}$$

where the sloshing moments Ω_{sx} and Ω_{sy} are linearly parameterisable, R is a characteristic dimension of the tank (*e.g.*, radius), and $\mathcal{K}_{\text{ij}}$ is a parameter related to the sloshing stiffness or frequency.

2.1.2 Modelling Changing Mass Effect

The liquid discharge dynamics are modelled by:

$$\begin{cases}\dot{m}_l(t) &= -k_c \rho_l S_n h_l(t) \\ m_l(t) &= m_0 - k_c S_n \rho_l \int_{t_0}^{t_f} h_l(t)\,\text{dt}\end{cases} \tag{9}$$

where $\dot{m}_l(t)$ is the rate of change of the liquid mass and $m_l(t)$ is the liquid mass at the time t. m_0 is the initial liquid mass at the time t_0, k_c is the discharge coefficient, S_n is the nozzle area, $h_l(t)$ is the fluid height, and ρ_l is the liquid's density. This captures the mass variation due to spraying, which influences both force and moment generation.

2.2 The Rotational Motion

The rotational dynamics of a quadrotor UAV are significantly influenced by the presence of a liquid payload, which introduces time-varying inertia and gravitational torque due to shifts in the centre of mass. The net inertia matrix is $I = I_q + I_l \in \mathbb{R}^{3\times3}$, where I_q is the constant inertia of the quadrotor, and I_l denotes the time-varying inertia due to the liquid payload.

The total torque about the centre of mass is given by:

$$\tau = \tau_a + r_{\text{ql}} \times R m_l(t)\, g \tag{10}$$

Here, τ_a is the aerodynamic torque, r_{ql} is the offset vector between the quadrotor and the liquid centre of mass, and g is the gravitational acceleration.

Applying Newton's second law of rotation and incorporating the effects of time-varying mass and inertia,

the angular acceleration becomes:

$$\begin{aligned}\dot{\omega}_b = &-\left(I_q+I_l\right)^{-1}\left[\omega_b\times\left(\left(I_q+I_l\right)\omega_b\right)\right]-\left(I_q+I_l\right)^{-1}\\ &\left[\dot{m}_l\left(t\right)\left(r_{\mathrm{ql}}^T r_{\mathrm{ql}}E_0-r_{\mathrm{ql}}r_{\mathrm{ql}}^T\right)\omega_b+\dot{I}_{\mathrm{ol}}\omega_b\right] \qquad (11)\\ + &\quad \left(I_q+I_l\right)^{-1}\tau_a+\left(I_q+I_l\right)^{-1}\left[r_{\mathrm{ql}}\times Rm_l\left(t\right)g\right]\end{aligned}$$

where ω_b is the angular velocity in the body frame, and $\dot{I}_{\mathrm{ol}}$ accounts for the liquid's own inertia dynamics. The aerodynamic torque is decomposed as $\tau_a = \tau_t + \tau_0 + \tau_s$, with $\tau_t = \begin{bmatrix}\tau_\phi & \tau_\theta & \tau_\psi\end{bmatrix}^T$ being the control torques, τ_0 other aerodynamic effects, and τ_s from liquid sloshing.

Assuming the inertia matrix I is diagonal, and the small-angle approximation holds ($\phi, \theta \approx 0$), the final simplified rotational dynamics [10] in Euler angles are:

$$\begin{aligned}\begin{bmatrix}\ddot{\phi}\\ \ddot{\theta}\\ \ddot{\psi}\end{bmatrix} = &\, I^{-1}\begin{bmatrix}\dot{\theta}\dot{\psi}\left(I_y-I_z\right)\\ \dot{\phi}\dot{\psi}\left(I_z-I_x\right)\\ \dot{\phi}\dot{\theta}\left(I_x-I_y\right)\end{bmatrix}+I^{-1}\begin{bmatrix}\tau_\phi\\ \tau_\theta\\ \tau_\psi\end{bmatrix}-I^{-1}\dot{I}\begin{bmatrix}\dot{\phi}\\ \dot{\theta}\\ \dot{\psi}\end{bmatrix}\\ &+I^{-1}\left(\tau_0+\tau_s+m_l\left(t\right)r_{\mathrm{ql}}\times \mathrm{Rg}\right) \qquad (12)\end{aligned}$$

3. Model Analysis

In this section, the earlier derived mathematical model is reformulated to enhance its applicability for controller design. To facilitate this, the translational dynamics of the quadrotor are expressed in a control-affine form. This reformulation incorporates the effects of liquid sloshing forces, time-varying mass, and external disturbances. The resulting expressions enable the use of virtual control inputs [10] u_{1x}, u_{1y}, and u_{1z}, which are defined as:

$$\begin{aligned}\ddot{x} &= -\tfrac{\dot{m}_l}{M}\dot{x}+\tfrac{1}{M}\left(u_{1x}+\Delta_{1x}\right)+d_x\\ \ddot{y} &= -\tfrac{\dot{m}_l}{M}\dot{y}+\tfrac{1}{M}\left(u_{1y}+\Delta_{1y}\right)+d_y\\ \ddot{z} &= -\tfrac{\dot{m}_l}{M}\dot{z}+\tfrac{1}{M}u_{1z}+d_z \qquad (13)\end{aligned}$$

where Δ_{1x} and Δ_{1y} denote sloshing effects; d_x, d_y, and d_z represent external disturbances. This formulation simplifies their integration into the subsequent nonlinear control framework, and R_1, R_2, and R_3 are the first three rows of the rotation matrix R. These are given as:

$$\begin{cases}u_{1x} = \left(c\left(\phi\right)s\left(\theta\right)c\left(\psi\right)+s\left(\phi\right)s\left(\psi\right)\right)u_1,\\ \quad \Delta_{1x} = R_1^T F_s, \quad d_x = R_1^T F_0/M\ ,\\ u_{1y} = \left(c\left(\phi\right)s\left(\theta\right)s\left(\psi\right)-s\left(\phi\right)c\left(\psi\right)\right)u_1,\\ \quad \Delta_{1y} = R_2^T F_s, \quad d_y = R_2^T F_0/M\ ,\\ u_{1z} = c\left(\phi\right)c\left(\theta\right)u_1, \quad d_z = -g+\frac{R_3^T F_0}{M}.\end{cases} \qquad (14)$$

where F_s is the sloshing force, and F_0 is an external force. The translational motion can be represented in a second-order state-space form:

$$\Sigma_i: \begin{cases}\dot{\xi}_{2i-1} = \xi_{2i}, \quad \mathrm{i}=1\ldots,3\\ \dot{\xi}_{2i} = f_i\left(\xi_r\right)+g_i\left(u_i+\Delta_i\left(\xi_r\right)\right)+d_i\left(\xi_r,t\right)\\ y_i = \xi_{2i-1}\end{cases} \qquad (15)$$

where $\xi_r = \left[\xi_1,\xi_2,\xi_3,\xi_4,\xi_5,\xi_6\right]^T = \left[x,\dot{x},y,\dot{y},z,\dot{z}\right]^T$, $f_i\left(\cdot\right) = -\frac{\dot{m}_l}{M}\xi_{2i}$, $g_i = \frac{1}{M}$, and $\Delta_i\left(\xi_r\right)$ represent the effects of sloshing forces. For rotational dynamics, using (12), the equations become:

$$\begin{aligned}\ddot{\phi} &= -\tfrac{\dot{I}_x}{I_x}\dot{\phi}+\tfrac{\dot{\theta}\dot{\psi}\left(I_y-I_z\right)}{I_x}+\tfrac{1}{I_x}\left(\tau_\phi+\Delta_\phi\right)+d_\phi\\ \ddot{\theta} &= -\tfrac{\dot{I}_y}{I_y}\dot{\theta}+\tfrac{\dot{\phi}\dot{\psi}\left(I_z-I_x\right)}{I_y}+\tfrac{1}{I_y}\left(\tau_\theta+\Delta_\theta\right)+d_\theta \qquad (16)\\ \ddot{\psi} &= -\tfrac{\dot{I}_z}{I_z}\dot{\psi}+\tfrac{\dot{\phi}\dot{\psi}\left(I_z-I_x\right)}{I_z}+\tfrac{1}{I_z}\tau_\psi+d_\psi\end{aligned}$$

This can be written in state-space form [10]:

$$\Sigma_i: \begin{cases}\dot{\xi}_{2i-1} = \xi_{2i}, \quad \mathrm{i}=1\ldots,3\\ \dot{\xi}_{2i} = f_i\left(\xi_\omega\right)+g_i\left(\tau_i+\Delta_i\left(\xi_\omega\right)\right)+d_i\left(\xi_\omega,t\right)\\ y_i = \xi_{2i-1}\end{cases} \qquad (17)$$

where $\xi_\omega = \left[\xi_1,\xi_2,\xi_3,\xi_4,\xi_5,\xi_6\right]^T = \left[\phi,\dot{\phi},\theta,\dot{\theta},\psi,\dot{\psi}\right]^T$ and $f\left(\xi_\omega\right) = \left[f_\phi, f_\theta, f_\psi\right]^T$. The nonlinear terms $f_i(\xi_\omega)$ are given by $f_\phi = -\frac{\dot{I}_x}{I_x}\dot{\phi}+\frac{\dot{\theta}\dot{\psi}\left(I_y-I_z\right)}{I_x}$, $f_\theta = -\frac{\dot{I}_y}{I_y}\dot{\theta}+\frac{\dot{\phi}\dot{\psi}\left(I_z-I_x\right)}{I_y}$, and $f_\psi = -\frac{\dot{I}_z}{I_z}\dot{\psi}+\frac{\dot{\phi}\dot{\psi}\left(I_z-I_x\right)}{I_z}$.

In sprayer quadrotor applications, sloshing effects are significant and compensated using a neural network (NN) identifier. Combining (15) and (17), the system is compactly expressed as:

$$\begin{cases}\dot{\xi}\left(t\right) = \mathrm{A}\xi\left(t\right)+B\left[f\left(\xi\right)+g\left(u+\Gamma\Delta\left(\xi\right)\right)+d\left(\xi,t\right)\right]\\ y = \xi\left(t\right)\end{cases} \qquad (18)$$

where $\xi = \left[x,\dot{x},y,\dot{y},z,\dot{z},\phi,\dot{\phi},\theta,\dot{\theta},\psi,\dot{\psi}\right]^T$, $f\left(\xi\right) = \left[f_x,f_y,f_z,f_\phi,f_\theta,f_\psi\right]^T$, A and B are coefficient matrices of appropriate dimensions, $f\left(\xi\right) = \begin{bmatrix}f_1\left(\xi\right) & f_2\left(\xi\right) & \cdots & f_p\left(\xi\right)\end{bmatrix}^T \in \mathbb{R}^{p\times 1}$, $g = \begin{bmatrix}g_1 & g_2 & \cdots & g_p\end{bmatrix}^T \in \mathbb{R}^{p\times p}$, $\Delta\left(\xi\right) = \begin{bmatrix}\Delta_1\left(\xi\right) & \Delta_2\left(\xi\right) & \cdots & \Delta_p\left(\xi\right)\end{bmatrix}^T \in \mathbb{R}^{p\times 1}$, and $\Gamma = \begin{bmatrix}\Gamma_1 & \Gamma_2 & \cdots & \Gamma_p\end{bmatrix}^T \in \mathbb{R}^{p\times p}$.

The goal is to design a controller u that stabilises (18) in the presence of sloshing effects $\Delta\left(\xi\right)$ and disturbances $d\left(\xi,t\right)$, while ensuring the state (t) tracks the reference y_r and all closed-loop signals remain UUB [29].

Assumption 3.1. *The control matrix g is invertible and norm-bounded such that $\leq \bar{g}_M$, where $\bar{g}_m$ and $\bar{g}_M$ are positive constants.*

Assumption 3.2. *The sloshing term $\Delta\left(\xi\right)$ and disturbance derivative $\dot{d}\left(\xi,t\right)$ are norm-bounded: $\| \Delta\left(\xi\right) \| \leq \bar{Q}_M$, and $\| \dot{d}\left(\xi,t\right) \| \leq \bar{d}_M$, for positive constants $\bar{Q}_M$ and $\bar{d}_M$.—*

Assumption 3.3. *The reference signal $y_r(t) \in \mathbb{R}^n$ is known and bounded with bounded derivatives.*

Remark 3.1. *While Assumption 3.1 may be strong, it ensures controllability and is critical for deriving a feasible control strategy. Assumptions 3.2 and 3.3 ensure system stability under bounded disturbances and tracking requirements.*

To facilitate controller design, the tracking error is defined as:

$$\dot{z}(t) = \mathrm{A}z(t) + F_z + \mathrm{B}g(u + \Gamma\Delta(\xi)) + \mathrm{B}d(\xi, t) \quad (19)$$

where $(t) = \xi(t) - y_r(t)$ and $F_z = \mathrm{B}f(\xi) - (\dot{y}_r - Ay_r)$. Based on (19), a suitable composite controller is developed for the system in the subsequent sections.

4. Construction of a Composite Controller

To estimate sloshing effects in a compact domain, an NN identifier is employed:

$$\Delta(\xi) = W^T\phi(\xi) + \epsilon(\xi) \quad (20)$$

Here, $W \in \mathbb{R}^{\updownarrow \times p}$ is the NN weight matrix, and $\updownarrow$ is the neuron number. $\phi(\xi) \in \mathbb{R}^{\updownarrow}$ is the NNs activation function, $\epsilon(\xi)$ is a bounded NN reconstruction error, and $\phi(\xi)$ and W are norms bounded by $\bar{\phi}_M$ and $\bar{W}$, respectively. The sloshing estimation error is given by $\widetilde{\Delta}(\xi) = \Delta(\xi) - \widehat{\Delta}(\xi)$, where $\Delta(\xi)$ is the ideal sloshing effect, and $\widehat{\Delta}(\xi)$ is the estimated sloshing effect. Note that a sigmoid activation function of the form $\phi_j(\xi) = \frac{2}{1+exp(-V_{\mathrm{ok}}x)} - 1$ is employed in the approximation, where $\phi_j(\xi)$ is the j-th element of $\phi(\xi)$, and V_{ok} is the k-th row of the constant weighted matrix $V_o \in \mathbb{R}^{\updownarrow \times n}$.

In this study, a sigmoid activation function is employed owing to its universal approximation capability and differentiability, which jointly enable stable weight adaptation in online learning. Specifically, its bounded output ensures robustness against significant input variations, while the smooth gradient facilitates efficient computation of weight updates within Lyapunov-based stability analysis frameworks [30]. These properties make it suitable for estimating dynamic sloshing forces in real-time UAV control applications.

Substituting into the system dynamics gives:

$$\dot{z}(t) = \mathrm{A}z(t) + F_z + \mathrm{B}g\left(u + W^T\phi(\xi)\right) + D(\xi, t) \quad (21)$$

where $D(\xi, t) = \mathrm{B}d(\xi, t) + Bg\epsilon(\xi)$ is the lumped disturbances. A DO is designed as follows to estimate the lumped disturbances:

$$\begin{cases} \widehat{D}(\xi, t) = \Lambda(z(t) - \xi(t)) \\ \dot{\xi}(t) = \mathrm{A}z(t) + F_z + \mathrm{B}g\left(u + \widehat{W}^T\phi(\xi)\right) + \widehat{D}(\xi, t) \end{cases} \quad (22)$$

where $\widehat{W}$ is the estimate of W. Λ is a positive-definite diagonal matrix, and $\| \Lambda^{-1} \| = \alpha_1$. Note that the disturbance estimation error e_d can be decreased by increasing the diagonal values of Λ. Meanwhile, according to Assumption 3.2, the derivative of $d(\xi, t)$ is norm bounded according to Assumption 3.2., *i.e.*, $\| \dot{D}(\xi, t) \| \leq \delta_M$. Thus, for large values of Λ, α_1 becomes relatively small such that $\alpha_1^2\delta_M^2$ reduces appreciably. Then, by defining the estimation errors as $e_d = D(\xi, t) - \widehat{D}(\xi, t)$ and $\widetilde{W} = W - \widehat{W}$, the disturbance error dynamics can be obtained as:

$$\begin{cases} \dot{z}(t) = \mathrm{A}z(t) + F_z + \mathrm{B}g\left(u + W^T\phi(\xi)\right) + D(\xi, t) \\ \dot{e}_d = -\Lambda e_d - \Delta\mathrm{B}g\widetilde{W}^T\phi(\xi) + \dot{D}(\xi, t) \end{cases} \quad (23)$$

So, the controller is:

$$u = u_s + u_o \quad (24)$$

where u_o is the nominal adaptive PI controller and u_s is the SMC.

The integral sliding surface is defined as:

$$\begin{aligned} \mathcal{S}(z) = \Pi\Big[&\mathcal{S}_1(z) - \mathcal{S}_1(0) - \int_0^t \mathcal{H}(\mathrm{A}z(t) + F_z \\ &+ \mathrm{B}gu_o)\,\mathrm{d}\tau\Big], \\ \text{with} \Xi_1 = \Pi\mathcal{H}&\mathrm{B}g. \end{aligned} \quad (25)$$

Here, $\partial\mathcal{S}_1(z)/\partial z = \mathcal{H}$. Here, $\mathcal{H} \in \mathbb{R}^{n\times n}$ and $\Pi \in \mathbb{R}^{n\times n}$ is a constant symmetric positive-definite matrix. Note that $\mathcal{S}_1(z)$ can be chosen as $\mathcal{S}_1(z) = z \in \mathbb{R}^n$ such that $\partial\mathcal{S}_1(z)/\partial z$ is a pure identity matrix.

Using the observer and NN identifier, the controller becomes:

$$\begin{aligned} u_s = &-\widehat{W}^T\phi(\xi) - \widehat{\mathcal{R}}\mathrm{sgn}\left(\mathcal{S}^T\Xi_1\right) \\ - &\quad \Xi_2\Pi\mathcal{H}\widehat{D}(\xi, t) - K_s\mathcal{S} \end{aligned} \quad (26)$$

Remark 4.1. *With $\mathcal{H} = I$, the term $(\mathbb{I} - \Xi_1\Xi_2)\Pi\mathcal{H}D(\xi, t) \to 0$, simplifying:*

$$\begin{aligned} \dot{\mathcal{S}}(z) = &\Xi_1\widetilde{W}^T\phi(\xi) + \Xi_1\Xi_2\Pi\mathcal{H}e_d \\ &- \Xi_1\widehat{\mathcal{R}}\mathrm{sgn}\left(\mathcal{S}^T\Xi_1\right) - \Xi_1K_s\mathcal{S} \end{aligned} \quad (27)$$

The new signal defines:

$$\mathcal{R}_b = \Xi_2\Pi\mathcal{H}e_d \quad (28)$$

Remark 4.2. *It is noted that $\mathcal{R}_b$ cannot be calculated directly since $D(\xi, t)$ is unavailable. However, from Assumption 3.2, it can be concluded that $\mathcal{R}_b$ is a bounded signal. To estimate $\mathcal{R}_b$, the robust feature of the sliding surface can be explored. Let $\widehat{\mathcal{R}}$ be the estimate of $\mathcal{R}_b$ and define the estimation error as $\widetilde{\mathcal{R}} = \bar{\mathcal{R}}_b - \widehat{\mathcal{R}}$, where $\bar{\mathcal{R}}_b \geq 0$ is the constant unknown bound of $\mathcal{R}_b$.*

Following Remark 4.2, the signal $\widehat{\mathcal{R}}$ is generated as follows:

$$\dot{\widehat{\mathcal{R}}} = \alpha_o\left(\sum_{i=1}^{p}\left|\left(\mathcal{S}^T\Xi_1\right)_i\right| - \lambda_b\widehat{\mathcal{R}}\right), \quad \alpha_o, \lambda_b > 0 \quad (29)$$

Theorem 4.1. *Consider system equation* (18) *with controller equation* (26) *and update law in* (30)*. The error signals $\mathcal{S}$, e_d, $\widetilde{W}$, and $\widetilde{\mathcal{R}}$ are UUB. The weight tuning of the NNs identifier is constructed as follows:*

$$\dot{\widehat{W}} = \Gamma_n\left(\phi(\xi)\mathcal{S}^T\Xi_1 + n_1\widehat{W}\right) \quad (30)$$

where $\Gamma_n \in \mathbb{R}^{\updownarrow\times\updownarrow}$ is a proper positive-definite diagonal matrix and $n_1 > 0$. Further, the DO is designed using (22) and the coupled error dynamics are considered as in (23). If

the controller is designed as (26), then the sliding surface $\mathcal{S}$, the disturbance estimation error e_d, the weight estimation error $\widetilde{W}$, and the error signal $\widetilde{\mathcal{R}}$ are UUB around the neighbourhood of zero. Additionally, the ultimate bounds can be decreased appreciably through proper choice of Λ, Π, n_1, and λ_b.

Lyapunov Function (Proof of Theorem 4.1):

$$L_1 = \frac{1}{2}\mathcal{S}^T\mathcal{S} + \frac{1}{2}e_d^T\Lambda^{-1}e_d + \frac{1}{2}\mathrm{tr}\left(\widetilde{W}^T\Gamma_n^{-1}\widetilde{W}\right) + \frac{1}{2}\alpha_o^{-1}\widetilde{\mathcal{R}}^2 \quad (31)$$

The derivative $\dot{L}_1$ is upper bounded by:

$$\dot{L}_1 \leq -\parallel \Xi_1 K_s \parallel\parallel \mathcal{S} \parallel^2 - C_1 \parallel e_d \parallel^2 - C_2 \parallel \widetilde{W} \parallel^2 - \frac{\lambda_b}{2}\bar{\mathcal{R}}_b^2 + \Delta \quad (32)$$

where $C_1 = 1/2\ + \bar{\phi}_M^2/2\ \rho$, $C_2 = \bar{g}_M^2/2\ \rho\ + n_1/2$, and $\Delta = 1/2\ \alpha_1^2\delta_M^2 + n_1/2\ \bar{W}^2$.

The outside is a compact set:

$$\parallel \mathcal{Z} \parallel > \sqrt{\frac{\Delta}{\lambda_{\min}(Q)}} \quad (33)$$

Which implies that the sliding surface $\mathcal{S}(z)$ and the estimation errors $e_d, \widetilde{W}$, and $\widetilde{\mathcal{R}}$ are UUB, since $\bar{\phi}_M, \bar{g}_M, n_1$, and δ_M are bounded positive constants. Considering (29), it is found that $\widehat{\mathcal{R}}$ is convergent, ensuring that u_s in (26) remain bounded. This completes the proof of Theorem 4.1.

Remark 4.3. *Theorem 4.1 depicts that the integral sliding surface* (25) *and DO* (22) *ensures UUB stability, although exact convergence* $\mathcal{S}(z) = 0$ *is impractical. With appropriate parameter selection* $\Lambda, K_s, \Pi,\ n_1$, *and* λ_b, *the effects of* δ_M *and* $\bar{W}$ *are minimised, and all errors converge near zero as* $t \to \infty$. *To avoid chattering introduced by* $\mathrm{sgn}(\cdot)$ *function in* (26), *a thin boundary layer using based on* $\arctan\left(\mathcal{S}^T\Xi_1(z)/\iota\right)$ *is applied, where* ι *is a small constant.*

The next step involves designing u_o to achieve suboptimal tracking for the nominal system.

4.1 Adaptive PI-based Control Design for the Nominal System

When the SMC u_s compensates for disturbances and sloshing, the nominal error dynamics can be simplified to:

$$\dot{z} = \mathrm{A}z(t) + F_z + \mathrm{B}g u_o \quad (34)$$

Define an auxiliary error:

$$e_z = R_1 z(t) + R_2 \int_0^t z(t)\,\mathrm{d}\tau \quad (35)$$

where R_1 and $R_2 \in \mathbb{R}^{p\times n}$ are carefully chosen positive matrices. This leads to:

$$\dot{e}_z = (R_1 A + R_2) z(t) + R_1 F_z + R_1 \mathrm{B}g u_o \quad (36)$$

Assumption 4.2. *According to Theorem 4.1, the error signal* $z(t)$ *is bounded, since the sliding surface* $\mathcal{S}(z)$ *and the function* F_Z *have all been shown to be bounded. This permits the following strong assumption to be stated: the term* $(R_1 A + R_2) z(t) + R_1 F_z$ *is upper bounded by a positive constant* $\bar{a}_M$, *such that* $\parallel (R_1 A + R_2) z(t) + R_1 F_z \parallel \leq \bar{a}_M \parallel e_z \parallel$.

A PI-like controller is proposed as:

$$u_o = -(K_p(t) + K_1) R_1 z(t) - (K_I(t) + K_2)\int_0^t z(t)\,\mathrm{d}\tau \quad (37)$$

where $K_p(t) \in \mathbb{R}^{p\times p}$ and $K_I(t) \in \mathbb{R}^{p\times n}$ are time-varying proportional and integrator gains, and K_1, and K_2 are positive constant matrices of appropriate dimensions.

Remark 4.4. *Thus, four degrees of freedom for PI gain estimation can be obtained if* $K_p(t), K_I(t), K_1$, *and* K_2 *are selected independently. For simplification, let* $K_I(t) = K_p(t) R_2$, *and* $K_2 = K_1 R_2$. *Then:*

$$u_o = -(K_p(t) + K_1) e_z \quad (38)$$

Theorem 4.2. *Defining adaptive laws:*

$$K_p(t) = \varsigma_0\widehat{\Theta} - K_1, \quad \varsigma_0 \in \mathbb{R}^+$$
$$\dot{\widehat{\Theta}} = \Gamma_p\left(\varsigma_0 \parallel e_z \parallel^2 K_1 - \varsigma_1\widehat{\Theta}\right), \quad \varsigma_1 \in \mathbb{R}^+ \quad (39)$$

where $\Gamma_p \in \mathbb{R}^{p\times p}$ is a diagonal positive-definite matrix, and $\widehat{\Theta}$ is the estimate of Θ, with the estimation error given by $\widetilde{\Theta} = \Theta - \widehat{\Theta}$. If Assumption 4.2 is satisfied, then the errors $\widetilde{\Theta}$ and e_z are UUB, and the system tracking error $z(t)$ will converge around zero with a suitable selection of $R_1, R_2, \varsigma_0, \varsigma_1$.

Lyapunov Function (Proof of Theorem 4.2):

$$L_2 = \tfrac{1}{2}e_z^T e_z + \tfrac{1}{2}\mathrm{tr}\left(\widetilde{\Theta}^T\Gamma_p^{-1}\widetilde{\Theta}\right) \quad (40)$$

Its derivative leads to:

$$\begin{aligned}\dot{L}_2 &\leq -\vartheta_2 \parallel e_z \parallel^2 - \frac{\varsigma_1}{2} \parallel \widetilde{\Theta} \parallel^2 + \frac{\varsigma_1}{2}\vartheta_1^2 \\ &\leq -\lambda_{\min}(M_e) \parallel \mathcal{B}_e \parallel^2 + \frac{\varsigma_1}{2}\vartheta_1^2 \\ &\leq -\mathcal{K}L_2 + \mathcal{C}\end{aligned} \quad (41)$$

Here,

$$\mathcal{B}_e = \begin{bmatrix} e_z \\ \widetilde{\Theta}\end{bmatrix}, \quad M_e = \begin{bmatrix} \vartheta_2 & 0 \\ 0 & \frac{\varsigma_1}{2}\end{bmatrix}$$
$$\mathcal{K} = \lambda_{\min}(M_e), \quad \mathcal{C} = \tfrac{\varsigma_1}{2}\vartheta_1^2.$$

By integrating (41),

$$0 \leq L_2 \leq \frac{\mathcal{C}}{\mathcal{K}} + \left(L_2(0) - \frac{\mathcal{C}}{\mathcal{K}}\right)\exp^{-\mathcal{K}t}. \quad (42)$$

From (42), it is clear that the ultimate convergence of L_2 is guaranteed, *i.e.*, $\lim_{t\to\infty} L_2 = \frac{\mathcal{C}}{\mathcal{K}}$, which means that the auxiliary error e_z and the parameter estimation error $\widetilde{\Theta}$ are stable in the sense of UUB. Thus, according to (38), the nominal controller u_o is also bounded. Finally, since e_z is UUB, it can then be concluded that the tracking error $z(t)$ is bounded and converges around the neighbourhood of zero, where the ultimate convergence can be guaranteed by properly tuning the parameters $\varsigma_0, \varsigma_1, R_1$, and R_2. This completes the proof of Theorem 4.2.

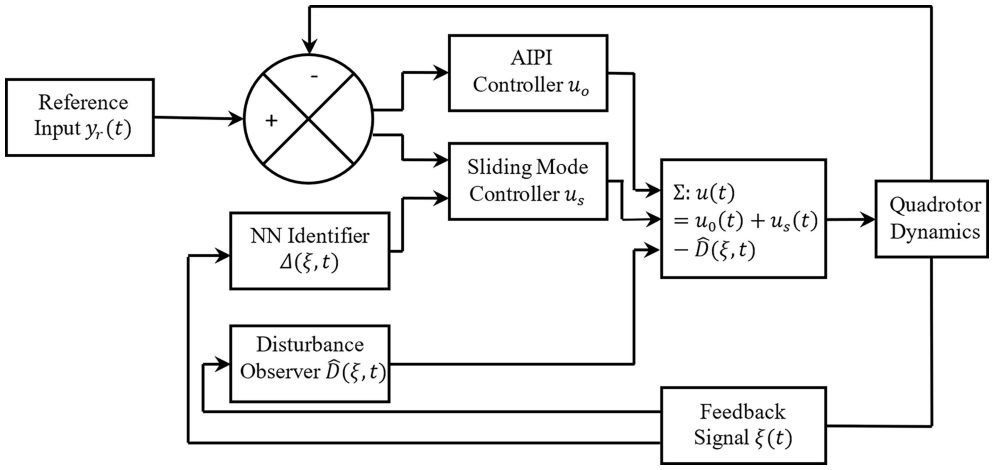

Figure 2. Block diagram of the control loop.

The overall control law is as follows:

$$\begin{aligned} u &= u_s + u_o \\ &= -\widehat{W}^T \phi(\xi) - \widehat{\mathcal{R}} \mathrm{sgn}\left(\mathcal{S}^T \Xi_1\right) - \Xi_2 \Pi \mathcal{H} \widehat{D}(\xi, t) - K_s \mathcal{S} \\ &- \left(K_p(t) + K_1\right) e_z \end{aligned} \tag{43}$$

Theorem 4.3. *For the error dynamics in* (19)*, the DO is designed as in* (22)*, and the sliding-mode sloshing accommodation as in* (25)*. The adaptive controller for the overall closed-loop system is given in* (43)*. The update laws for the NN identifier and that of the PI-based design are provided in* (30) *and* (39)*, respectively. By utilising the basic assumptions (1–4), it is shown that all signals in the closed-loop system remain stable in the sense of UUB, and the tracking error* $z(t)$ *converges to a small neighbourhood near the origin.*

Lyapunov Function (Proof of Theorem 4.3):

$$L = L_1 + L_2 \tag{44}$$

Based on Theorems 4.1 and 4.2, the equation is derived as:

$$\dot{L} \leq -\lambda_{\min}(\Pi_z) \parallel \bar{X} \parallel^2 + \bar{\Delta}_p \tag{45}$$

It is then found that $\dot{L}$ is negative if $\parallel \bar{X} \parallel > \sqrt{\frac{\bar{\Delta}_p}{\lambda_{\min}(\Pi_z)}}$ which means all the signals in the vector $\bar{X}$ are UUB. From (35) and (38), the boundedness of e_z ensures that $u_o, \int_0^t z(t)\, d\tau$, and $z(t)$ remain bounded. As $z(t) = \xi - y_r$, it suggests that ξ is also a bounded signal and hence F_z and $\dot{z}$ in (34) are all bounded. Moreover, it is evident from (45) that the ultimate bound of e_z can be arbitrary small if the parameters α_1, n_1, and ς_1 are appreciably small enough. This implies that the tracking error $z(t)$ converges to small neighbourhood around zero as $t \to \infty$. Hence, the proof of Theorem 4.3 is complete.

5. Numerical Study

5.1 Parameters

In this section, numerical simulations of the developed strategy are carried out to evaluate the effectiveness of the proposed adaptive robust control scheme. To verify this scheme, simulations were performed using MATLAB R2016b. The control architecture, including the DO, NN identifier, and controllers, is illustrated in Fig. 2, and the physical parameters of the liquid carrier UAV are presented in Table 1.

The corresponding system matrices related to the parameters in (18) are defined as follows:

$$A_r = A_\omega = \begin{bmatrix} 0&1&0&0&0&0 \\ 0&0&0&0&0&0 \\ 0&0&0&1&0&0 \\ 0&0&0&0&0&0 \\ 0&0&0&0&0&1 \\ 0&0&0&0&0&0 \end{bmatrix}, \quad B_r = B_\omega = \begin{bmatrix} 0&0&0 \\ 1&0&0 \\ 0&0&0 \\ 0&1&0 \\ 0&0&0 \\ 0&0&1 \end{bmatrix},$$

$$\mathrm{A} = \begin{bmatrix} A_r & 0_{6\times 6} \\ 0_{6\times 6} & A_\omega \end{bmatrix}, B = \begin{bmatrix} B_r & 0_{6\times 3} \\ 0_{6\times 3} & B_\omega \end{bmatrix},$$

$x_d = cos(0.5t)$ m, $z_d = 1 + t$ m, $\psi_d = 0.5$ rad, $\phi_d = \tan^{-1}\left(\left(\frac{u_{1x}}{u_{1z}} - tan(\theta_d)\cos(\psi)\right)\frac{\cos(\theta_d)}{\sin(\psi_d)}\right)$

$$\theta_d = \frac{(u_{1x}\cos(\psi) + u_{1y}\sin(\psi))}{u_{1z}},$$

$$\mathrm{y}_d = \begin{cases} 2, & \text{if} \quad 0 \leq t < 10 \\ 1, & \text{if} \quad 10 \leq t < 20 \\ 2, & \text{otherwise} \end{cases}, \phi, \theta \in \left(-\frac{\pi}{2} - \delta, \frac{\pi}{2} + \delta\right)$$

for small $\delta > 0$.

Table 1
Parameters of the Liquid Carrier Quadrotor UAV [4]
System

Parameters	**Values**	**Unit**
Mass	12	kg
Arm length	22.5	cm
Vertical distance	20	cm
Moment of inertia	1.5, 1.5, 3	kgm^2
Gravity	9.8	ms^{-2}
Rotor inertia	0.003	$\text{kg}m^2$
Rotor angular velocity	0.03	$\text{rad}s^{-1}$
Length	36	cm
Width	36	cm
Height	36	cm
Mass	5	kg
Density of the liquid	1002	$\text{kg}m^3$
Sloshing frequency	0.2∼0.4	$\text{rad}s^{-1}$

The initial translational position and velocity vector are given as $\xi_r = [0.2, -0.2, 2, 2, 0.2, 0]^T$ and angular position and angular rate vector are $\xi_\omega = [-0.1, 0, 0.3, 0.2, 0.1, 0.2]^T$. According to the composite control design, parameters chosen are: $\Lambda = 15\mathbb{I}_{n\times n}$, $\alpha_o = 10$, $\lambda_b = 0.7$, $\mathcal{H} = \mathbb{I}_{n\times n}$, $\widehat{\mathcal{R}}(0) = 0$, $n_1 = 0.5$, and $\Gamma_n = 3 \times 10^{-3}\mathbb{I}_{\updownarrow\times\updownarrow}$. $V_0 \in \mathbb{R}^{\updownarrow\times n}$ and the initial value of $\widehat{W} \in \mathbb{R}^{\updownarrow\times p}$ are randomly selected within the interval $[0, 1]$, with $p = 6, n = 12,$ and $\updownarrow = 11$. $K_s = \text{rand}(6, 12)$ and $\Pi = \mathbb{I}_{12\times 12}$ are chosen as the sliding gain and identity matrix. The parameters for the adaptive PI-based nominal controller are selected as $\varsigma_0 = 14\mathbb{I}_{p\times p}$, $\varsigma_1 = 1.8 \times 10^{-3}\mathbb{I}_{p\times p}$, $\widehat{\Theta}(0) = 0\mathbb{I}_{p\times p}$, $R_1 = 20 * \text{rand}(6, 12)$, $R_2 = 2 * \text{rand}(6, 12)$, and $K_1 = 7 * \text{rand}(6, 6)$.

Sloshing loads were employed in the body frame as sinusoidal inputs: forces $F_{s,x} = -0.128\sin(0.4t)$ N, $F_{s,y} = -0.024\sin(0.2t)$ N and torques $\tau_{s,x} = -0.046\sin(0.4t)$Nm, $\tau_{s,y} = 0.08\sin(0.2t)$ Nm. Aerodynamic/rotor translational disturbance used $V_a = 2\ \text{ms}^{-1}$, $b = 0.3$ rad, $F_{h1..4} = \{1.2, 2.3, 4.1, 1.6\}$ N, $\rho_a = 1.2\ \text{kg}m^{-3}$, $S_a = 0.4\ m^2$, $C_{\text{xy}} = 0.2$, $C_z = 0.1$, yielding $d_r = F_h + F_d \approx [8.606, 2.662, 0.096]^\top$ N. Rotor-hub/gyroscopic torque disturbance used $J_r = 0.003\ \text{kg}m^2$, $\Omega_r = 400\ s^{-1}$, $p = 0.3$, $q = 0.4$, giving $\tau_0 \approx [-0.064, 1.398, 0.343]^\top$ Nm. Disturbance scheduling matched the plotted cases: in the x–y translation channels, $d_x = d_{r,x}$for $0 \le t < 15$ s then a 1 N bias; $d_y = 0$ for $0 \le t < 5$ s, $d_y = d_{r,y}$for $5 \le t < 15$ s, then 1 $N + 0.3$ $N\exp(-2t)$. In attitude, θreceived $\tau_{0,y}$ and ψ received $\tau_{0,z}$ over $0 \le t < 15$ s, then a 1Nm bias (or 1 Nm$+$ 0.3 Nm$\exp(-2t)$). The payload mass decreased according to $\dot{m} = -k_c\rho S_n h_\updownarrow$ with $k_c = 0.08$ and $S_n = 1 \times 10^{-6}\ m^2$.

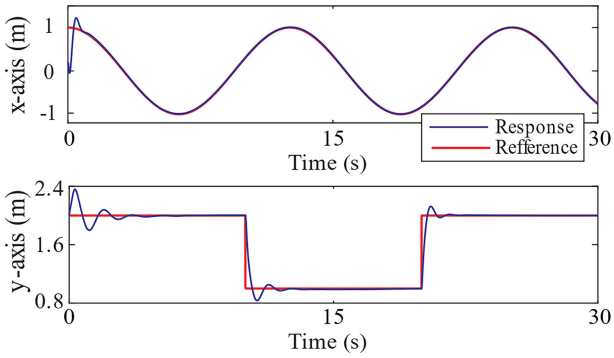

Figure 3. Time response of the quadrotor's X and Y positions in the presence of external disturbances.

6. Results

The performance of the proposed adaptive robust controller was evaluated in MATLAB using a plant protection quadrotor model that incorporates liquid sloshing dynamics. The simulation results cover trajectory tracking, sloshing disturbance rejection, and a comparative analysis with a PID controller. The complete set of simulations is available in an online repository [31] for future research and development purposes. The trajectory tracking results demonstrate the tracking performance of the proposed controller as shown in Figs. 3–6. Figures 3 and 4 illustrate the positional tracking response of the quadrotor under the influence of external disturbances and varying liquid mass, while the overall control architecture, including the DO, NN identifier, and controllers, is depicted in Fig. 2. Figure 5 demonstrates the rotational motion response and 3D tracking performance is illustrated in Fig. 6. It obvious that the proposed controller provides a good response capabilities, confirming that the measured states ξ closely track the desired signals y_d in the presence of disturbances. As presented in Fig. 4, small peaks occur at $t = 10$ s and $t = 25$ s due to the changing liquid mass (from 5 kg to 3 kg to 1 kg) in the tank; however, the trajectory converges quickly to reference signal, depicting that the proposed control scheme works well to guarantee the stability of the system despite the presence of the changing liquid mass.

6.1 Trajectory Tracking

6.2 Controller Response to Sloshing Effects

From Fig. 7, it can be observed that the sloshing forces $F_{s,x}$ and $F_{s,y}$ are estimated accurately by the NN identifier, while the sloshing moments $\tau_{s,x}$ and $\tau_{s,y}$ are compensated by the nonlinear DO. This shows that the NN identifier can be regarded as an effective scheme for detecting liquid sloshing. Furthermore, the effect of the sloshing moments in the angular rates has also been effectively eliminated, as seen in Fig. 8. The effects of sloshing and controller's reaction can further be observed in the sliding surfaces as shown in Fig. 9. Likewise, the adaptive robust controllers shown in Fig. 10 illustrate how the main thrust u_1 together with the torques u_φ, u_θ, and u_ψ works to

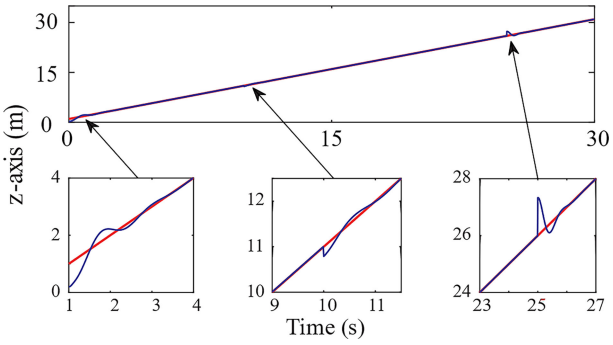

Figure 4. Time response of quadrotor's z position in the presence of changing mass and external disturbances.

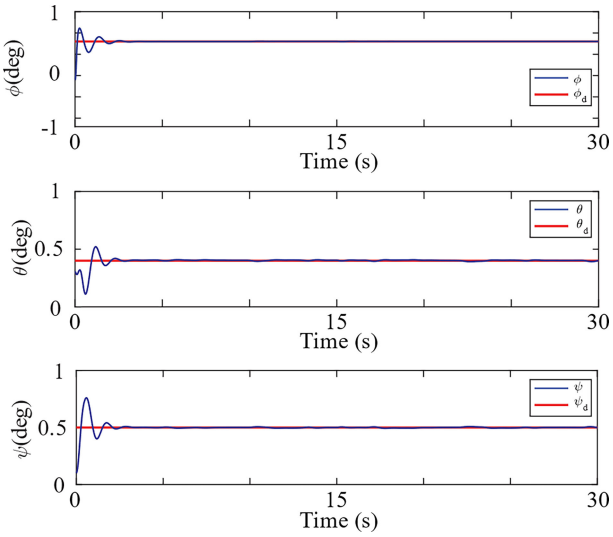

Figure 5. Time response of the quadrotor roll, pitch, and yaw in the presence of external disturbances.

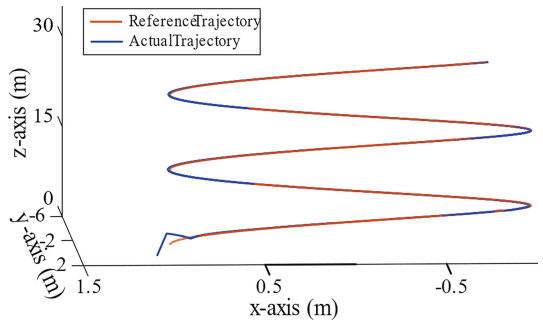

Figure 6. 3D path tracking of the quadrotor using the proposed control scheme for attitude and position control under external disturbances and changing liquid mass.

regulate the changes in altitude and the variations due to liquid sloshing. Finally, the convergence of the parameters of the proposed adaptive PI-based nominal controller is presented in Fig. 11.

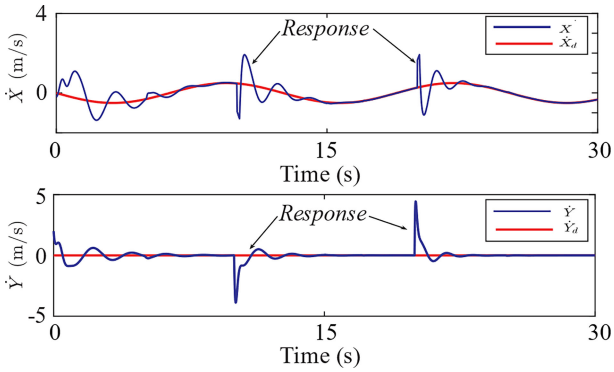

Figure 7. Time response of the quadrotor's X and Y velocities in the presence of sloshing forces.

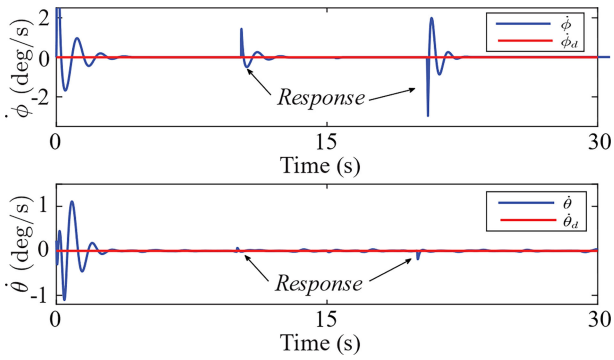

Figure 8. Time response of the quadrotor's roll and pitch rates in the presence of sloshing moments.

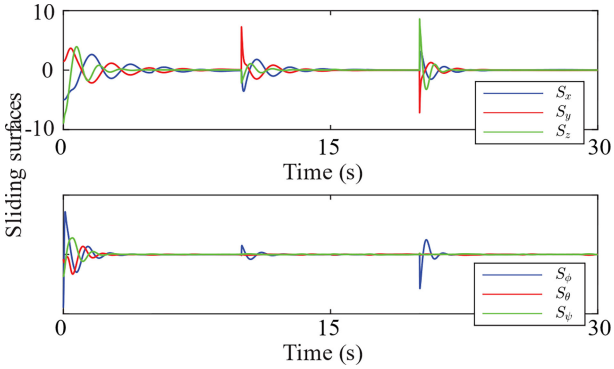

Figure 9. Sliding surfaces concerning the positions and orientations.

6.3 Comparison with PID Controller

To further demonstrate the effectiveness of the proposed adaptive robust controller, its tracking performance is compared with that of a PID controller using the experimental setup. The integral absolute error (IAE), defined as $\mathrm{IAE}\,(\Sigma_i) = \int_0^t |E_i|\,\mathrm{d}\tau$ is used to summarise the tracking performance of the two controllers, where $E_i = \sqrt{z_{i,1}^2 + z_{i,2}^2 + \ldots + z_{i,n_i}^2}$. For translational motion, $n_i = 6$, with $i = 1, 2, 3$ for the subsystems $\ddot{x}, \ddot{y}$, and $\ddot{z}$, respectively. Similarly, for the rotational motion $n_i = 6$ with $i = 1, 2, 3$ for the subsystems $\ddot{\phi}, \ddot{\theta}$, and $\ddot{\psi}$, respectively. In the absence

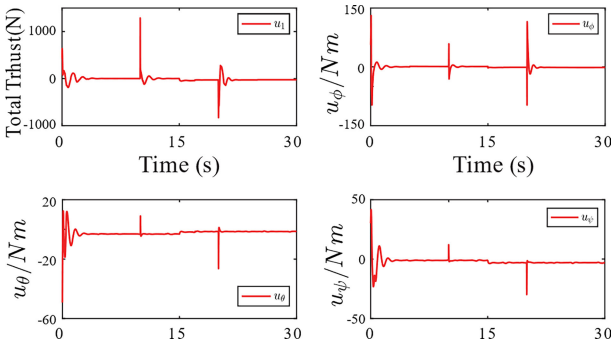

Figure 10. The control inputs of quadrotor in the presence of sloshing forces and external disturbances.

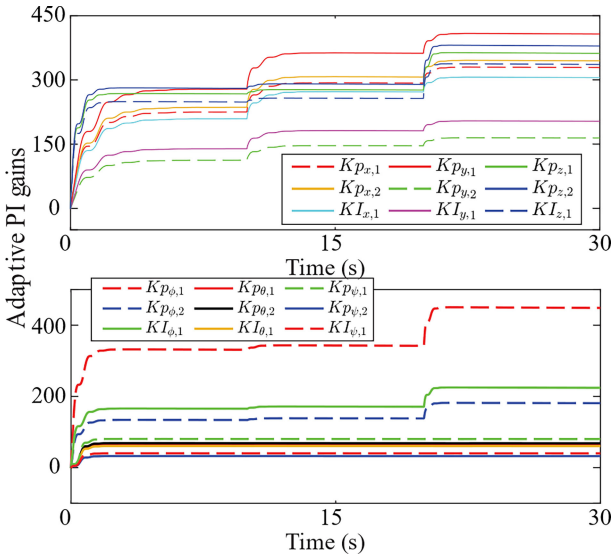

Figure 11. Adaptive gains of the PI controller.

of sloshing forces and a zero-mass rate, the proposed scheme guarantees superior tracking performance. For clarity of the results, the tracking performance of both control schemes is illustrated in Fig. 12. It can also be observed that the angular positions depict nearly equal performance for both the proposed and PID controllers. This is particularly due to the fact that the sloshing effect mainly affects in the translational motion rather than rotational motion. In addition, as sloshing in the z-direction was set to zero; both the controllers exhibit similar tracking performance in the z-direction.

For liquid-carrying UAVs, integral tracking-error indices (*e.g.*, IAE) function as stability indicators because they capture both transient and steady deviations under persistent, state-dependent disturbances. Among comparable studies, each tackle only one side of the liquid problem while benchmarking against classical baselines. The ISA SMC [28] focuses time-varying mass and compares it to a PD controller, reporting rapid closure, very high attitude accuracy, and severe overshoot/instability of PD under mass change. In contrast, the recent LQG [27] targets sloshing, compares to PID/PI controllers, and reports an overall reduction of the integral tracking-error norm from 0.59 (PID) to 0.47 (LQG) (∼20%),

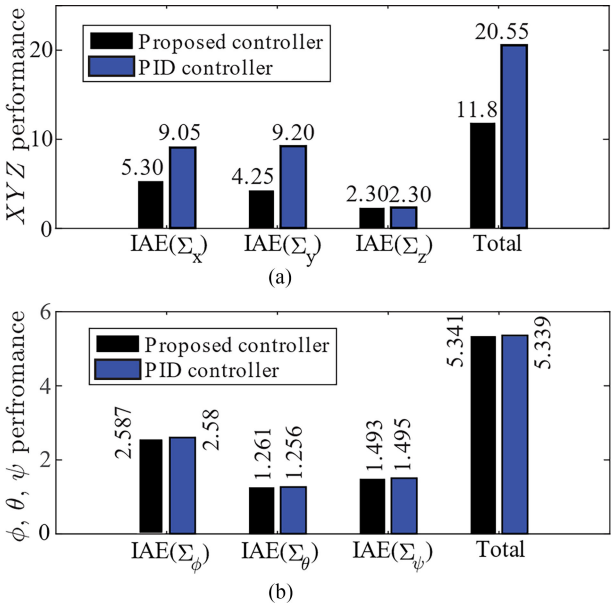

Figure 12. Comparison of the tracking performance of subsystems Σ_i among the proposed adaptive robust controller and a PID controller.

alongside lower actuation effort. Our composite AIPI-SMC addresses the practical, complex mixed-disturbance case by jointly compensating time-varying mass and internal slosh *via* integral sliding, DO, and NN slosh identifier. Against a well-tuned PID, it achieves ≈41.4% (x-axis) and ≈53.8% (y-axis) IAE reductions while maintaining comparable functionality in attitude channels. In short, whereas ISA SMC (versus PD) and LQG (versus PID/PI) excel effectively when each targets a single disturbance source, our presented model yields higher tracking-error gains in the mixed-disturbance regime, surpassing the tracking-error reduction record for LQG's.

7. Conclusion and Future Work

In the current study, an adaptive integral PI-based SMC (AIPI-SMC) was designed for stabilising agricultural sprayer quadrotor UAVs, which face dynamic disturbances from liquid sloshing and variable payloads during spraying operation and obstacle avoidance. Combining NN identification with a nonlinear DO, a mathematical model was designed for quadrotor UAVs with an attached liquid tank. A sigmoid activation function was employed in the NN to estimate the dynamic liquid slosh due to its universal approximation capability and differentiability, which together bound the output to ensure stable adaptation of weights in online learning. The bounded output improves robustness against significant input variations, while the smooth gradient facilitates efficient computation of weight updates within Lyapunov-based stability analysis frameworks. Based on this, a nonlinear DO is developed to effectively estimate external disturbances. By integrating these two observers, the AIPI-SMC was designed, and the PI-based controller stabilises the nominal system and improves trajectory tracking. Lyapunov-based stability proofs demonstrate

that the overall system errors remain bounded, ensuring robust trajectory tracking despite uncertainties. Numerical simulations demonstrate the effectiveness of the proposed controller in tracking performance and disturbance rejection, surpassing a conventional PID controller. Overall, the presented control strategy effectively maintains stability and robustness even under significant mass variations and liquid sloshing, making it highly applicable for agricultural UAV spraying operations. Future work will focus on experimental validation, including hardware-in-the-loop (HIL) and field flight experiments, and on extending the framework to more aggressive flight manoeuvres and larger payload variations.

Acknowledgement

The authors are grateful for the support of the National Key R&D Program (Project) of China: 2024YFD2300301.

References

[1] G. Farid, M. Hongwei, S. M. Ali, and Q. Liwei, A review on linear and nonlinear control techniques for position and attitude control of a quadrotor, *Mechatronic System and Control, 45*(1), 2017, 43–57.

[2] A. Jebelli, A. Najafiyanfar, A. Mahabadi, and M.C.E. Yagoub, Fault-tolerant control of a quadrotor despite the complete rotor failure, *International Journal of Robotics and Automation*, *39*(4), 2024, 258–269.

[3] G. Farid, H.W. Mo, A.H. Baqar, and S.M. Ali, Comprehensive modelling and static feedback linearization-based trajectory tracking control of a quadrotor UAV, *Mechatronic System and Control*, *46*(3), 2018, 97–106.

[4] S. Ahmed, B. Qiu, C.W. Kong, H. Xin, F. Ahmad, and J. Lin, A data-driven dynamic obstacle avoidance method for liquid-carrying plant protection UAVs, *Agronomy-Basel, 12*(4), 2022, 1–25.

[5] M.F.Q. Say, E. Sybingco, A.A. Bandala, R.R.P. Vicerra, and A.Y. Chua, A genetic algorithm approach to PID tuning of a quadcopter UAV model, in *Proceedings of IEEE/SICE International Symposium on System Integration (SII),* 2021, 675–678.

[6] L. Li, Z. Hu, Q. Liu, T. Yi, P. Han, R. Zhang, and L. Pan, Effect of flight velocity on droplet deposition and drift of combined pesticides sprayed using an unmanned aerial vehicle sprayer in a peach orchard, *Frontiers in Plant Science, 13*, 2022, 981494.

[7] M.C. Agurob, A.J. Bano, I. Paradela, S. Clar, E. R. Aleluya, and C.J. Salaan, Autonomous vision-based unmanned aerial spray system with variable flow for agricultural application, *IAENG International Journal of Computer Science, 50*(3), 2023, 1–16.

[8] S. Ahmed, H. Xin, M. Faheem, and B. Qiu, Stability analysis of a sprayer UAV with a liquid tank with different outer shapes and inner structures, *Agriculture-Basel, 12*(3), 2022, 1–18.

[9] A. Tayebi and S. McGilvray, Attitude stabilization of a VTOL quadrotor aircraft, *IEEE Transactions on Control Systems Technology, 14*(3), 2006, 562–571.

[10] F. Kendoul, Z.Y. Yu, and K. Nonami, Guidance and nonlinear control system for autonomous flight of minirotorcraft unmanned aerial vehicles, *Journal of Field Robotics, 27*(3), 2010, 311–334.

[11] S.M. Jiao, D.P. Liu, and X.K. Zheng, Attitude control of quadcopter based on self-tuning linear active disturbance rejection, *Mechatronic System and Control*, *46*(3), 2023, 102–109.

[12] S. Gonzalez-Vazquez and J. Moreno-Valenzuela, A new nonlinear PI/PID controller for quadrotor posture regulation, in *Proceedings of International Conference on Electronics, Robotics and Automotive Mechanics, CERMA*, 2010, 642–647.

[13] T. Madani and A. Benallegue, Backstepping control for a quadrotor helicopter, in *Proceedings of IEEE/RSJ International Conference on Intelligent Robots and Systems*, 2006, 3255–3260.

[14] E. Fresk and G. Nikolakopoulos, Full quaternion-based attitude control for a quadrotor, in *Proceedings of European Control Conference (ECC)*, 2013, 3864–3869.

[15] H. Boudjedir, O. Bouhali, and N. Rizoug, Adaptive neural network control based on neural observer for quadrotor unmanned aerial vehicle, *Advanced Robotics, 28*(17), 2014, 1151–1164.

[16] H. Wang, Z. Li, H. Xiong, and X. Nian, Robust H ∞ attitude tracking control of a quadrotor UAV on SO(3) via variation-based linearization and interval matrix approach, *ISA Transactions, 87,* 2019, 10–16.

[17] M. Chen and W.H. Chen, Sliding mode control for a class of uncertain nonlinear system based on disturbance observer, *International Journal of Adaptive Control and Signal Processing, 24*(1), 2010, 51–64.

[18] V.K. Tripathi, S.C. Yogi, A.K. Kamath, L. Behera, N.K. Verma, and S. Nahavandi, A disturbance observer-based intelligent finite-time sliding mode flight controller design for an autonomous quadrotor, *IEEE Systems Journal, 16*(1), 2022, 1649–1660.

[19] H. Maqsood and Y.H. Qu, Nonlinear disturbance observer based sliding mode control of quadrotor helicopter, *Journal of Electrical Engineering & Technology, 15*(3) 2020, 1453–1461.

[20] M. Izadi and R. Faieghi, High-gain disturbance observer for robust trajectory tracking of quadrotors, *Arxiv,* 2024, 105854.

[21] F. Chen, F. Lu, B. Jiang, and G. Tao, Adaptive compensation control of the quadrotor helicopter using quantum information technology and disturbance observer, *Journal of the Franklin Institute-Engineering and Applied Mathematics, 351*(1), 2014, 442–455.

[22] C. Diao, B. Xian, B. Zhao, X. Zhang, and S. Liu, An output feedback attitude tracking controller design for quadrotor unmanned aerial vehicles using quaternion, in *IEEE/RSJ International Conference on Intelligent Robots and Systems*, 2013, 3051–3056.

[23] R. Zhang, Q. Quan, and K.Y. Cai, Attitude control of a quadrotor aircraft subject to a class of time-varying disturbances, *IET Control Theory and Applications, 5*(9), 2011, 1140–1146.

[24] Y. Yang, J. Wu, and W. Zheng, Variable structure attitude control for a UAV with parameter uncertainty and external disturbance, *Procedia Engineering, 15,* 2011, 408–415.

[25] J. Zhang, H. Xu, D. Zhang, and D. Liu, Safety modeling and simulation of multi-factor coupling heavy-equipment airdrop, *Chinese Journal of Aeronautics, 27*(5), 2014, 1062–1069.

[26] J.O. Pedro, A. Panday, and L. Dala, A nonlinear dynamic inversion-based neurocontroller for unmanned combat aerial vehicles during aerial refuelling, *International Journal of Applied Mathematics and Computer Science, 23*(1), 2013, 75–90.

[27] A. Soltani and A. Vahidi Bajestani, Linear quadratic Gaussian control for a liquid-carrying quadrotor, *Iranian Journal of Science and Technology, Transactions of Electrical Engineering, 48*(1), 2024, 395–408.

[28] X. Wu, B. Xiao, and Y. Qu, Modeling and sliding mode-based attitude tracking control of a quadrotor UAV with time-varying mass, *ISA Transactions, 124,* 2019, 436–443.

[29] M. Han, Y. Tian, L. Zhang, J. Wang, and W. Pan, Reinforcement learning control of constrained dynamic systems with uniformly ultimate boundedness stability guarantee, *Automatica*, *129*, 2021, 109689.

[30] M. Pizzoli, F. Saltari, F. Mastroddi, J. Martinez-Carrascal, and L.M. González-Gutiérrez, Nonlinear reduced-order model for vertical sloshing by employing neural networks, *Nonlinear Dynamics*, *107*(2), 2022, 1469–1478.

[31] S. Ahmed, Mathematical modeling and flight controller design for liquid carrier agricultural sprayer UAV using varying mass and liquid slosh. [Repository], https://github.com/shibbir7ahmed/Quadrotor-controller-design-using-varying-mass-and-liquid-slosh (accessed 25 March 2025).

Biographies

Shibbir Ahmed received the Doctorate degree in agricultural engineering from the College of Agricultural Engineering, Jiangsu University, China. He is currently working with the College of Agriculture, Yangzhou University, China. His major research directions are smart agriculture and precision farming.

Muhammad Yousaf Nadeem received the Doctorate degree in crop science from the College of Agriculture, Nanjing Agricultural University, China. He is currently working with the College of Agriculture, Yangzhou University, China. His major research directions are smart agriculture, crop physiology, and precision farming.

Muhammad Zain received the Doctorate degree in agriculture from the Chinese Academy of Agricultural Sciences, China. He is currently a Postdoctoral Researcher with North China University of Water Resources and Electric Power, China. His major research direction is precision agriculture.

Zubair Iqbal received the Doctorate degree in agriculture from the Chinese Academy of Agricultural Sciences, China. He is currently a Postdoctoral Researcher with the Memorial University of Newfoundland, Canada. His major research directions are crop genetics and crop physiology.

Issac Tawiah is currently pursuing a Doctoral degree with the Department of Automation and Perception, Shanghai Jiao Tong University, China. His research interests include remote sensing, artificial intelligence, and smart agriculture.

Chengming Sun received the Doctorate degree in crop science from the College of Agriculture, Yangzhou University, China. He is currently a Professor with the Institute of Smart Agriculture, College of Agriculture, Yangzhou University. His research interests include remote sensing, artificial intelligence, and smart agriculture.